EVALUATION OF DISTORTION CORRECTION OF DIFFUSION-WEIGHTED MR IMAGES OF HUMAN CERVIX

*Maysam Jafar, Sharon Giles, Veronica Morgan, Maria Schmidt, Martin O. Leach, Nandita M. deSouza

CRUK and EPSRC Cancer Imaging Centre,
Institute of Cancer Research & Royal Marsden NHS Foundation Trust, Surrey SM2 5NG. UK

ABSTRACT

Diffusion-weighted images are increasingly being employed in conjunction with T2-weighted images for accurate diagnosis of cervical cancer. However, these images suffer from eddy-current related and magnetic field inhomogeneity induced distortions. This paper presents an investigation into the reverse gradient technique to correct distortions in diffusion-weighted echo-planar images of human cervix. We hypothesize that the correction aligns the diffusion-weighted images with the T2-weighted images. To allow for any misalignments and to evaluate the correction, a normalized cross-correlation driven template matching strategy was employed to assess the correlation between the corrected image and the T2-weighted image. For $b = 0 smm^{-2}$ images, mean correlation values of 0.72 ± 0.14 for regions-of-interest drawn around the cervix for 10 patients were achieved. We also found that our hypothesis was most valid in regions encompassing the cervix with a misalignment of $4.4 \pm 3.4 mm$. Results are presented for images acquired at a field-of-view of $100 mm$ using an endovaginal coil developed in-house for cervix imaging at 3T which is the first of its kind in the world.

Index Terms— EPI Distortion Correction, Reverse Gradient

1. INTRODUCTION

Cervical cancer is the third most common gynaecological cancer in women and it accounts for one in ten cancers diagnosed in women worldwide [1]. Because of its soft tissue contrast, magnetic resonance imaging (MRI) is the modality of choice employed in diagnosis and staging of cervical cancer [2]. Diffusion-weighted MRI (DW-MRI) has been employed to further improve the detection of small cervical tumours because of significantly lower apparent diffusion coefficient (ADC) of cervical tumour compared to normal cervical tissue [3]. However, DW-MRI suffers from two types of distortions, firstly, magnetic field inhomogeneity induced distortions in an EPI-based (Echo-Planar Imaging) sequence where residual eddy-currents cause translation, shear, and scaling [4] and secondly, eddy-current related distortions caused by strong diffusion-sensitizing magnetic field gradients which have short ramp times. The latter depends on the magnitude and direction of the diffusion encoding field gradients. These combined image distortions are worst in the phase-encode direction and therefore spatial distortions along the phase-encoding axis will be several orders of magnitude larger than those along the frequency-encoding axis. Several approaches have been proposed to correct for such distortions. Most of these methods were devised to correct for EPI-based distortions and were later extended to diffusion-weighted EPI-based sequences. These can be further classified into phase-based [5] and image-based techniques [6][7][8], all of which were applied to the human brain. Phase-based techniques yield good corrections but they suffer from increased acquisition time.

In this paper we focus on an image-based technique referred to as the reverse gradient technique proposed by Chang and Fitzpatrick [9] and aim to investigate its applicability in correcting distortions in diffusion images of the cervix and assess its performance in correcting features.

2. MATERIALS AND METHODS

In this work, we hypothesize that the correction algorithm is an alignment procedure such that pixel locations in the corrected image are aligned with those in the T2W image. To account for any misalignment, we employed normalized cross-correlation (NCC) in a template matching strategy. We chose NCC because it assumes a linear relationship between intensities and we are interested in features which maintain this relationship. This enables us to evaluate the degree of similarity using the highest correlating points calculated by template matching as well as the assessment of our alignment hypothesis using the l^2 norm between the T2-weighted which in this case acts as our ground truth and the corrected image.

2.1. Reverse Gradient

Reverse gradient technique was originally proposed to correct for field inhomogeneity induced artefacts in standard spin-echo images [9]. The technique requires the acquisition of

*maysam.jafar@icr.ac.uk

two images of the same object under the same conditions except for the polarity of the frequency-encode line. This means that the spatial shifting in the images from the two acquisitions will occur in opposite directions. The spatial shifting in the second image occurs along the frequency-encode line compared with the first image. The pair of two-dimensional images can be treated as a collection of independent pairs of one-dimensional images one for each value of the frequency-encode line. If one can determine some initial x_{10} in the first image $i_1(x_1)$ corresponding to some x_{20} in the second image $i_2(x_2)$ by setting a boundary condition then one can find x_1 for every x_2 such that integrals along a frequency-encode line remain equal. This condition is demonstrated in equation 1.

$$\int_{x_{10}}^{x_1} i_1(\zeta_1)d\zeta_1 = \int_{x_{20}}^{x_2} i_2(\zeta_2)d\zeta_2 \tag{1}$$

The corrected position x in the profile of interest and corrected intensity $i(x)$ can then be obtained by equations 2 and 3 respectively:

$$x = \frac{x_1 + x_2}{2} \tag{2}$$

$$i(x) = \frac{2i_1(x_1)i_2(x_2)}{i_1(x_1) + i_2(x_2)} \tag{3}$$

The corrected image is generated from the combination of both distorted forward and reverse gradient images and therefore it is expected that it will exhibit a signal-to-noise ratio which is higher than either of the distorted images [7]. In our application this method is applied along the phase-encode (left-right) axis as distortions along phase-encode axis are several orders of magnitude larger than those along the frequency-encode axis for a single shot EPI-based sequence.

2.2. Template Matching by Normalized Cross-Correlation

We used a normalized cross-correlation template matching approach as defined in Gonzalez [10]. For every pixel (p, q) in images A and B, a kernel k is centred at position (p, q) in image A and a neighbourhood t positioned at (p, q) in image B to define the search area. The highest matching coordinate $(p + p', q + q')$ is found in image B by maximizing the normalised cross correlation O as defined in equations 4 and 5 with respect to relative translation (a, b) within search neighbourhood t of image B. The offset values p' and q' are assigned to $\overrightarrow{C}(p, q)$, reflecting the maximum correlating position with respect to the current point (p, q).

$$O(p,q,a,b) = \frac{\sum_{i,j}[k(p+i,q+j) - \bar{k}(p,q)][t(a+i,b+j) - \bar{t}(a,b)]}{\left(\sum_{i,j}[k(p+i,q+j) - \bar{k}(p,q)]^2 \sum_{i,j}[t(a+i,b+j) - \bar{t}(a,b)]^2\right)^{\frac{1}{2}}} \tag{4}$$

$$\overrightarrow{C}(p,q) = \max_{a,b}[O(p,q,a,b)] \tag{5}$$

In equations 4 and 5, k defines the kernel window, $(p - \lfloor k/2 \rfloor) \leq i \leq (p + \lfloor k/2 \rfloor)$ and $(q - \lfloor k/2 \rfloor) \leq j \leq (q + \lfloor k/2 \rfloor)$ define the kernel surrounding, t defines the neighbourhood to be searched, $(p - \lfloor N/2 \rfloor) \leq a \leq (p + \lfloor N/2 \rfloor)$ and $(q - \lfloor N/2 \rfloor) \leq b \leq (q + \lfloor N/2 \rfloor)$ define the relative indices of the neighbourhood where N defines the size of the neighbourhood and $(\lfloor . \rfloor)$ defines the lower bound operator. The mean intensities of k and t are denoted by $\bar{k}$ and $\bar{t}$ respectively.

2.3. Error Metric

Given the availability of ground truth images $\overrightarrow{G}(p, q)$ as defined in 6, we chose to use the Euclidean distance metric or l^2 norm to measure the alignment error, expressed as the distance between the ground truth image and the corrected image. This is defined in equation 7 where $\overrightarrow{G}(p, q)$ and $\overrightarrow{C}(p, q)$ denote the ground truth data and the result of correlation respectively.

$$\overrightarrow{G}(p,q) = (p,q) \tag{6}$$

$$d(p,q) = \|\overrightarrow{G}(p,q) - \overrightarrow{C}(p,q)\|_2, (p,q) \in B^2 \tag{7}$$

where $d(p, q)$ denotes the Euclidean distance, B^2 denotes the set of points within the image or within a region-of-interest (ROI) drawn on the image and $\|.\|_2$ denotes the l^2 norm.

2.4. Image Acquisition

A total of 10 patients with cervical cancer were recruited to the study and underwent endovaginal MRI with written informed consent under a protocol approved by our institutional research ethics committee. Imaging was performed on a 3.0T Philips Achieva MR system (Philips Healthcare, Best, the Netherlands). The endovaginal receiver coil was developed in-house. A turbo spin-echo (SE) sequence was employed to acquire T2-weighted images in three planes orthogonal to the cervix. The chosen parameters were a field-of-view (FOV) of $100mm$, echo time $80ms$, repetition time $3400ms$, spectral pre-saturation inversion recovery fat suppression (SPIR), left-right phase encoding, 2 averages, acquisition matrix 238×238, $0.42mm$ in-plane resolution, image matrix 288×288, $0.35mm$ resolution, 24 slices with $2mm$ slice thickness and $0.1mm$ separation. The diffusion-weighted images were acquired coronal to the cervix using a single shot SE EPI-based sequence. The chosen parameters were a FOV of $100mm$, echo time $52ms$, repetition time $8000ms$, SPIR fat suppression, left-right phase encoding, 1 average, acquisition matrix 80×80, $1.25mm$ in-plane resolution, image matrix 224×224, b-values of 0, 100, 300, 500 and $800smm^{-2}$, 24 slices with $2mm$ slice thickness and $0.1mm$ separation. A left-right phase encoding was chosen as opposed to an anterior-posterior to avoid distortions through the cervix. The long repetition time in the diffusion sequence was due to the extra suppression pulses added to improve the quality of the acquired images.

2.5. Post-processing

Diffusion images were resized to the size of the T2W images. In the computation of both reverse gradient correction and template matching only $b = 0smm^{-2}$ and $b = 800smm^{-2}$ images were considered where no diffusion sensitization gradients are applied in the acquisition of the $b = 0smm^{-2}$ images and the largest diffusion gradients are applied in the acquisition of the $b = 800smm^{-2}$ (compared with other b values). The significance of the $b = 0smm^{-2}$ image is that it has the highest signal-to-noise ratio whilst the $b = 800smm^{-2}$ image has the lowest signal-to-noise but highlights abnormality within tissue clearly due to diffusion restriction.

Template matching utilizing normalized cross-correlation (NCC) as defined in equations 4 and 5 for $b = 0$ and $b = 800smm^{-2}$ images was computed for the three central slices of each patient as this captured most cervix features. We chose image A to be the corrected diffusion image with a kernel k of size 25 $\times$ 25 pixels ($8.8mm \times 8.8mm$) and image B to be the T2-weighted image with a search neighbourhood t of 51 $\times$ 51 pixels ($18mm \times 18mm$) . The l^2 norm distance measure as defined in equation 7 was then computed between pixel locations in the T2W image, assumed to be the ground truth, and each of the corrected $b = 0$ and $b = 800smm^{-2}$ images. Regions-of-interest were defined as those encompassing the cervix. These were drawn around each patient independently by an experienced observer. The mean NCC value across all slices of all patients was then used to provide a quantitative assessment of the overall image similarity and the mean distance was used to give the overall alignment error. This was then repeated for ROIs drawn by the observer around the cervix for each patient.

3. RESULTS

Reverse, forward, corrected and T2W $b = 0smm^{-2}$ images for a coronal slice through the centre of the cervix for one of the patients, are shown in Fig.1. In Fig.2, a correlation map of the coronal slice for the same patient (shown in Fig.1), is shown. An ROI encompassing the cervix is also shown. There is a significant correlation in the ROI encompassing the cervix between the T2W image and the diffusion image. The mean NCC across the ROI was 0.71$\pm$0.10 compared with a mean value of 0.57$\pm$0.15 across the entire slice (Fig.2).

The mean distance for the entire volume for both $b = 0smm^{-2}$ and $b = 800smm^{-2}$ images, was found to be 6.2$\pm$3.2mm and 6.7$\pm$3.0mm respectively (Table 1). Both $b = 0smm^{-2}$ and $b = 800smm^{-2}$ images yielded similar alignment errors despite the large diffusion gradients in the case of $b = 800smm^{-2}$ images compared to $b = 0smm^{-2}$. This suggests that eddy-currents due to large diffusion gradients have minimal effect on image distortions and the majority of distortions are field inhomogeneity induced due to the EPI-based sequence and the cervix-air interface and the presence of the endovaginal receiver coil.

	$d_{b=0}mm$	$d_{b=800}mm$	NCC$_{b=0}$	NCC$_{b=800}$
VOL	6.2$\pm$3.2	6.7$\pm$3.0	0.57$\pm$0.16	0.56$\pm$0.15
ROI	4.4$\pm$3.4	5.4$\pm$3.4	0.72$\pm$0.14	0.70$\pm$0.13

Table 1. Mean and standard deviation of l^2 norm d, and normalized cross-correlation (NCC). Values shown across the entire volume (VOL) and regions-of-interest (ROI) for the three central slices of all patients for both $b = 0smm^{-2}$ and $b = 800smm^{-2}$ images.

An NCC of 0.57$\pm$0.16 for $b = 0smm^{-2}$ and 0.56$\pm$0.15 for $b = 800smm^{-2}$ images was obtained signifying that good correlation is achieved between features in the T2W and the diffusion images. Misalignment decreased for pre-defined ROIs. This resulted in a mean misalignment of 4.4$\pm$3.4mm for the $b = 0smm^{-2}$ and 5.4$\pm$ 3.4mm for the $b = 800smm^{-2}$ images. The mean NCC across all ROIs also increased and was computed to be 0.72$\pm$0.14 for the $b = 0smm^{-2}$ and 0.70$\pm$0.13 for the $b = 800smm^{-2}$ images. Correlation values were lower for the $b = 800smm^{-2}$ images compared with $b = 0smm^{-2}$, likely because of lower signal-to-noise ratio due to the application of large diffusion gradients. The best correlation values were achieved in regions with homogenous tissues.

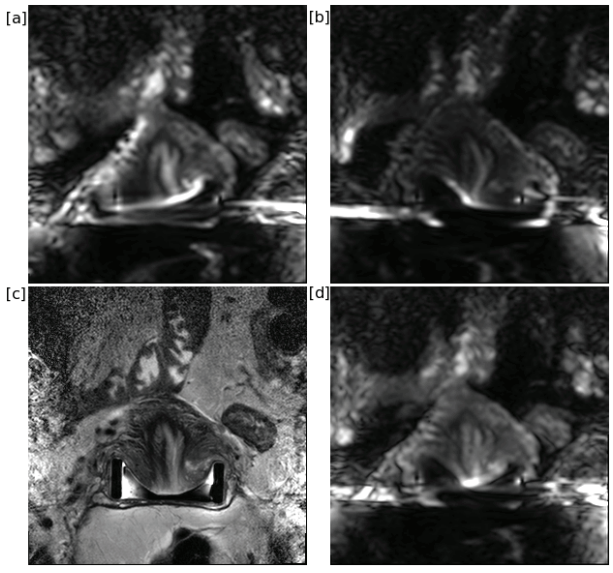


Fig. 1. Coronal slice through the centre of the cervix. (a) Reverse gradient $b = 0smm^{-2}$ (b) Forward gradient $b = 0smm^{-2}$ (c) T2W (d) Corrected $b = 0smm^{-2}$ images at a field-of-view of $100mm$.

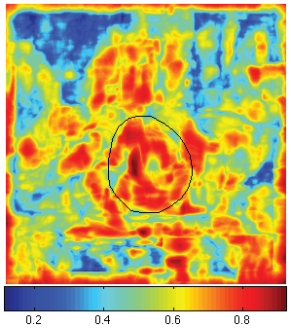


Fig. 2. Normalized cross-correlation (NCC) map for the same slice as in Fig.1 between the T2W (Fig.1c) and corrected b = $0smm^{-2}$ (Fig.1d). A region-of-interest (ROI) is drawn around the cervix. The mean correlation across the entire slice is 0.57±0.15 and in the ROI is 0.71±0.10.

4. CONCLUSIONS

Previous attempts to correct for spatial distortions in diffusion-weighted images using the reverse gradient technique focused on human brain. In this paper spatial distortions on human cervix images were corrected using the reverse gradient technique. Two sets of reversed polarity diffusion images, as well as T2-weighted, were acquired with an endovaginal coil developed in-house at 3T which is the first of its kind in the world. It was hypothesized that the correction technique yielded images which were aligned with the T2-weighted images. To test the alignment, template matching using normalized cross-correlation was utilized to assess the similarity between the distortion corrected diffusion images and the T2W images. The maximum error found within the region-of-interest was $5.4\pm3.4mm$ for the b = $800smm^{-2}$ images. This is within the chosen sizes of the kernel k ($8.8mm$) and neighbourhood t ($18mm$). Clearly, correlating either the forward or reverse gradient images with the T2W image will result in lower correlation than that of corrected and T2W, in particular in regions encompassing the cervix. Experienced observers found the corrected images better for diagnosis than either polarities.

Future work will include implementation of the correction algorithm in a clinical setting. Alternative correcttion techniques will be sought as the extra acquisition is inconvenient for the patient. We also plan to further enhance the alignment using misalignments found in this work. The variability of features from one acquisition to the next is also a problem which is particularly evident in slices closest to the bladder. It is our intention to assess feature tracking techniques which are invariant to scale and orientation. Correcting distortion in diffusion-weighted images particulary at high field strengths such as 3T remains a challenging problem due to increased magnetic field inhomogeneity and this is still an area of active research.

5. ACKNOWLEDGEMENTS

We acknowledge the support received from CRUK and EPSRC Cancer Imaging Centre in association with the MRC and Department of Health (England) grant C1060/A10334, also NHS funding to the NIHR Biomedical Research Centre. We would also like to thank Dr. Geoffrey Payne and Dr. Matt Orton at the Royal Marsden, Sutton.

6. REFERENCES

[1] CRUK, "Stats Team (June 2011) CencerStats Key Facts Cervical Cancer, Technical Report, Cancer Research UK," 2011, Cervical cancer statistics - Key Facts.

[2] NM. deSouza, GA. McIndoe, WP. Soutter, T. Krausz, KM. Chui, C. Hughes, and WP. Mason, "Value of Magnetic Resonance Imaging with an Endovaginal Receiver Coil in the Preoperative Assessment of Stage I and IIa Cervical Neoplasia," *British Journal of Obstetrics and Gynaecology*, vol. 105(5), pp. 500–7, 1998.

[3] E. M. Charles-Edwards, C. Messiou, V. A. Morgan, S. S. De Silva, N. A. McWhinney, M. Katesmark, A. D. Attygalle, and N. M. deSouza, "Diffusion-Weighted Imaging in Cervical Cancer with an Endovaginal Technique: Potential Value for Improving Tumor Detection in Stage Ia and Ib1 Disease," *Radiology*, vol. 249, no. 2, pp. 541–550, Nov. 2008.

[4] P. Jezzard and R. S. Balaban, "Correction For Geometric Distortion In Echo-planar Images From B-0 Field Variations," *Magnetic Resonance In Medicine*, vol. 34, no. 1, pp. 65–73, July 1995.

[5] P. Jezzard, A. S. Barnett, and C. Pierpaoli, "Characterization of and Correction for Eddy Current Artifacts in Echo Planar Diffusion Imaging," *Magnetic Resonance In Medicine*, vol. 39, no. 5, pp. 801–812, May 1998.

[6] N. Bodammer, J. Kaufmann, M. Kanowski, and C. Tempelmann, "Eddy Current Correction in Diffusion-Weighted Imaging using Pairs of Images Acquired with Opposite Diffusion Gradient Polarity," *Magnetic Resonance In Medicine*, vol. 51, no. 1, pp. 188–193, Jan. 2004.

[7] P. S. Morgan, R. W. Bowtell, D. J. O. McIntyre, and B. S. Worthington, "Correction of Spatial Distortion in EPI due to Inhomogeneous Static Magnetic Fields using the Reversed Gradient Method," *Journal of Magnetic Resonance Imaging*, vol. 19, no. 4, pp. 499–507, Apr. 2004.

[8] J. C. Haselgrove and J. R. Moore, "Correction for Distortion of Echo-Planar Images Used to Calculate the Apparent Diffusion Coefficient," *Magnetic Resonance In Medicine*, vol. 36, no. 6, pp. 960–964, Dec. 1996.

[9] H. Chang and J. M. Fitzpatrick, "A Technique for Accurate Magnetic-Resonance-Imaging in the Presence of Field Inhomogeneities," *IEEE Transactions On Medical Imaging*, vol. 11, no. 3, pp. 319–329, Sept. 1992.

[10] R. C. Gonzalez and R. E. Woods, *Digital Image Processing*, Prentice Hall, 2nd edition (2001).